Interpretation of Electron Delocalization in Benzene, Cyclobutadiene, and Borazine Based on Visualization of Individual Molecular Orbital Contributions to the Induced Magnetic Fiel...

ARTICLE *in* THE JOURNAL OF PHYSICAL CHEMISTRY A · JANUARY 2014

Impact Factor: 2.69 · DOI: 10.1021/jp411410r · Source: PubMed

3 AUTHORS:

Nickolas D Charistos
Aristotle University of Thessaloniki
14 PUBLICATIONS **29** CITATIONS
SEE PROFILE

Anastasios Papadopoulos
Aristotle University of Thessaloniki
13 PUBLICATIONS **21** CITATIONS
SEE PROFILE

M.P. Sigalas
Aristotle University of Thessaloniki
90 PUBLICATIONS **1,069** CITATIONS
SEE PROFILE

THE JOURNAL OF PHYSICAL CHEMISTRY A

Article

pubs.acs.org/JPCA

Interpretation of Electron Delocalization in Benzene, Cyclobutadiene, and Borazine Based on Visualization of Individual Molecular Orbital Contributions to the Induced Magnetic Field

Nickolas D. Charistos,* Anastasios G. Papadopoulos, and Michael P. Sigalas*

Department of Chemistry, Laboratory of Applied Quantum Chemistry, Aristotle University of Thessaloniki, Thessaloniki 54 124, Greece

Supporting Information

ABSTRACT: The magnetic response of the valence molecular orbitals (MOs) of benzene, cyclobutadiene, and borazine to an external magnetic field has been visualized by calculating the chemical shielding in two-dimensional grids of points on the molecular plane and on a plane perpendicular to it, using gauge-including atomic orbitals (GIAOs). The visualizations of canonical MO contributions to the induced magnetic field (CMO-IMF) provide a clear view of the spatial extension, the shape, and the magnitude of shielding and deshielding areas within the vicinity of the molecule, originating from the induced currents of each valence orbital. The results are used to investigate the delocalization of each valence MO and to evaluate its contribution to the aromatic character of systems under study. The differentiation of the total magnetic response among the three molecules originates exclusively from π-HOMO orbitals because the magnetic response of the subsets of the remaining MOs is found to be almost identical. Borazine is classified as nonaromatic as the four electrons that occupy the π-HOMO are found to be strongly localized on nitrogen centers. CMO-IMF can clarify the interpretation of various NICS indexes and can be applied for the investigation of various types of electron delocalization.

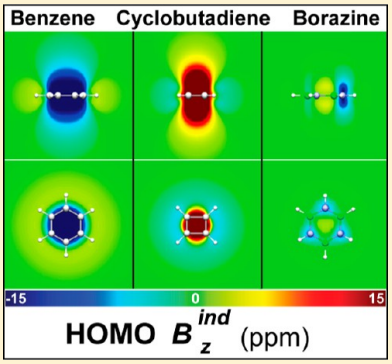

INTRODUCTION

Like many other concepts in chemical theory, aromaticity is a valuable tool used by chemists to classify chemical species, as well as to understand and predict chemical behavior. Aromatic molecules exhibit thermodynamic stability, special structural characteristics (planarity, high symmetry, and bond length equality), exceptional reactivity (substitution reactions), and characteristic spectroscopic properties (downfield proton NMR chemical shifts), all being a consequence of cyclic or spherical delocalization of valence electrons. Benzene, the archetypical paradigm of aromatic molecules, represents an ideal case of the concept of aromaticity, and it is profoundly described by Hückel theory.[1] However, in the last decades, the synthesis or the theoretical prediction of many peculiar species has expanded the notion of aromaticity to novel and exciting areas, such as metal aromaticity, Möbius aromaticity, three-dimensional aromaticity, and multiple aromaticity to name a few.[2,3] Today, almost a century and a half after its introduction to chemical thinking, the definition and measurement of aromaticity remains a controversial issue for chemical researchers. Thus, many theoretical qualitative and quantitative methods and indexes, based on energetic, structural, or magnetic criteria, have been developed in order to measure aromaticity. However, in many cases, these methods do not correlate with each other, and they usually have a narrow field of applicability, retaining aromaticity as a "fuzzy" concept without unique quantitative assessment.[4,5]

Methods based on magnetic criteria have been recognized as convenient tools for measuring aromaticity as they support the understanding of the concept of aromaticity by connecting electron delocalization with the magnetic response based on Pople's ring current model.[6] Cyclic electron delocalization affects the magnetic properties of aromatic molecules. When a uniform external magnetic field, $\mathbf{B}^{ext}$, is applied perpendicular to the molecular ring, it produces ring currents of mobile delocalized electrons. These currents induce a counter magnetic field, $\mathbf{B}^{ind}$, that presents a toroidal topology with opposite direction inside of the ring, diminishing (shielding) the external field, and with the same direction outside of the ring, reinforcing (deshielding) the external field. Proton magnetic resonance frequencies, which are experimentally obtained with respect to a reference compound by ^{1}H NMR spectroscopy as chemical shifts, are determined by the superposition of the external magnetic field, $\mathbf{B}^{ext}$, and the induced magnetic field, $\mathbf{B}^{ind}$, at the nucleus position. Hence, hydrogens inside of an aromatic ring experience a decreased field, leading to an upfield shift of the chemical shielding, while hydrogens outside of the ring experience an enhanced field, leading to a downfield shift of the chemical shielding. Thus, the experimental measurement of proton chemical shifts with NMR spectroscopy has been

Received: November 20, 2013
Revised: January 16, 2014

   dx.doi.org/10.1021/jp411410r | J. Phys. Chem. A XXXX, XXX, XXX−XXX

established as the most convenient analytical tool for the inspection of aromaticity in unsaturated organic molecules.

In recent years, a variety of qualitative and quantitative computational methods that calculate magnetic properties, related to either ring currents or the induced magnetic field, have been extensively applied to evaluate and depict aromaticity. The most popular among magnetic indexes is the nucleus-independent chemical shift (NICS),[7] owing its popularity to the simplicity of its calculation and its seemingly straightforward interpretation. Traditionally, NICS is the negative of the isotropic value of the chemical shielding tensor at the center of the molecular ring. Because chemical shielding is directly related to the induced magnetic field, large negative NICS values inside of the ring correspond to a strong diatropic field that characterizes aromatic molecules, while large positive NICS values inside of the ring stand for paratropic fields that characterize antiaromatic molecules. However, the reduction of a multifaceted property, such as the induced magnetic field, to a single value at a single point is problematic, and a superficial interpretation may lead to erroneous conclusions.[8−10]

The isotropic value, $NICS_{iso}$, contains in-plane contributions, corresponding to the magnetic response when the external field is applied parallel to the molecular ring. Thus, in order to recover the Pople's ring current model, it is clear that only the out-of-plane component of the nucleus-independent shielding tensor, $NICS_{zz}$, should be considered.[11] In addition, NICS indexes contain information from the magnetic response of all electrons. Contributions from localized core and σ electrons are significant at distances close to the molecular framework and obscure the contribution of the delocalized electrons. A crude approach to eliminate contributions from core and σ electrons is to calculate the chemical shielding at a distance about 1 Å above the ring,[12] where the magnetic response of these electrons is assumed to be negligible. However, this approach does not give any insight about the origin of the magnetic shielding, and it cannot be generally applied because different species may exhibit different local contributions in the same relative point, as, for example, in metallic systems.

The most convenient approach to resolve this issue is the dissection of NICS into orbital contributions, using either localized molecular orbitals (LMO-NICS) or canonical molecular orbitals (CMO-NICS). LMO-NICS[13] employs the IGLO[14] method together with the Pipek−Mezey localization procedure[15] to dissect the total shieldings into individual contributions from localized orbitals corresponding to individual chemical bonds. Thus contributions from the core, σ, and π orbitals can be separated. This method is effectively applicable to planar arenes, where the $NICS_{\pi zz}$ index was found to have the best correlation with other aromaticity indexes.[16] Alternatively, CMO-NICS[17] employs the gauge-including atomic orbital (GIAO)[18] formalism to dissect total shieldings into contributions from each MO. In this way, detailed information about the magnetic response of each orbital as well as of any compilation of orbitals can be derived. This method has a wide applicability as molecules presenting σ, multiple, metal, and 3D aromaticity have been studied.[19−22] Still, the interpretation of MO contributions may not be as straightforward as it seems. The application of CMO-NICS to [n]annulenes reveales that low-energy π and σ orbitals have significant diatropic contributions to the total NICS,[23] while only the frontier orbitals are expected to contribute to the induced ring currents.[24]

Various NICS indexes attempt to reduce all of the information of the three-dimensional magnetic field to a quantity referring to a single point in space. However, localized electrons present significant contributions to magnetic shielding at points close to the ring, while ring currents of delocalized electrons have long-range effects. Furthermore, ring currents of delocalized electrons are a much more complicated incident than the ideal circular electric currents of macroscopic devices, making thus precarious any conclusions about the magnetic response based on a single point in space. Hence, it is apparent that more information about the topology of the induced magnetic field is needed in order to draw reliable conclusions about the aromaticity of a system. In this context, many researchers have studied the chemical shielding function in space, calculating NICS in one-, two-, or three-dimensional grids.

Klod and Kleinpeter[25] calculated the chemical shielding in a three-dimensional grid of points surrounding the molecule, with dimensions 10 × 10 × 10 Å and a step of 0.5 Å. The results were visualized as isosurfaces of the isotropic shielding values, which are called iso-chemical-shielding surfaces (ICCSs), providing coherent qualitative information about the spatial extension, the sign, and the scope of the molecular magnetic response, corresponding to ring currents of aromatic rings as well as to anisotropic effects of double and triple bonds. Recently, Karadakov and Horner[26] calculated and visualized detailed isosurfaces and contour plots of the isotropic chemical shielding with a spacing of 0.05 Å. They used these visualizations not only to evaluate the aromaticity of systems such as benzene and cyclobutadiene but also to examine the influence of aromaticity on chemical bonds.

Merino et al.[27] directly related the shielding function to the induced magnetic field (IMF) by calculating its values in two and three dimensions and visualizing the results as vectors of the IMF and as isosurfaces or isocontour maps of its magnitude and its z-component, which is equivalent to $NICS_{zz}$. They showed that visualization of the IMF reveals the characteristic response of aromatic, antiaromatic, and nonaromatic molecules to an external field. Our team[28] performed similar calculations and visualizations of the magnetic response of triphenylene and its BN-substituted analogues and investigated the variation of local aromaticity of these systems. Recently Muñoz-Castro applied the same technique to investigate spherical aromaticity[29] and heavy elements rings.[30]

Heine et al.[31] proceeded with the dissection of the IMF into contributions from the core and σ and π subsets of orbitals, employing the LMO-NICS procedure, and investigated the aromaticity of a large series of planar molecules,[32] revealing in each case the shape and the spatial extension of diatropic and paratropic areas originating from π- and σ-electron delocalization. Although the LMO methodology allows the dissection of the IMF into contributions from single orbitals or orbitals with the same symmetry, Heine et al. analyzed the role of the total π and σ orbital subsets in aromaticity without providing information about the contribution of each individual orbital to the magnetic response. Therefore, additional insight about the origin of π- and σ-electron delocalization is still required, particularly in species where the degree of aromaticity is controversial, such as borazine,[33] or in systems presenting multiple types of delocalized electrons, such as radial aromatic species.[34]

In this study, we present the dissection of the IMF into contributions from individual canonical MOs, a method that

dx.doi.org/10.1021/jp411410r | J. Phys. Chem. A XXXX, XXX, XXX−XXX

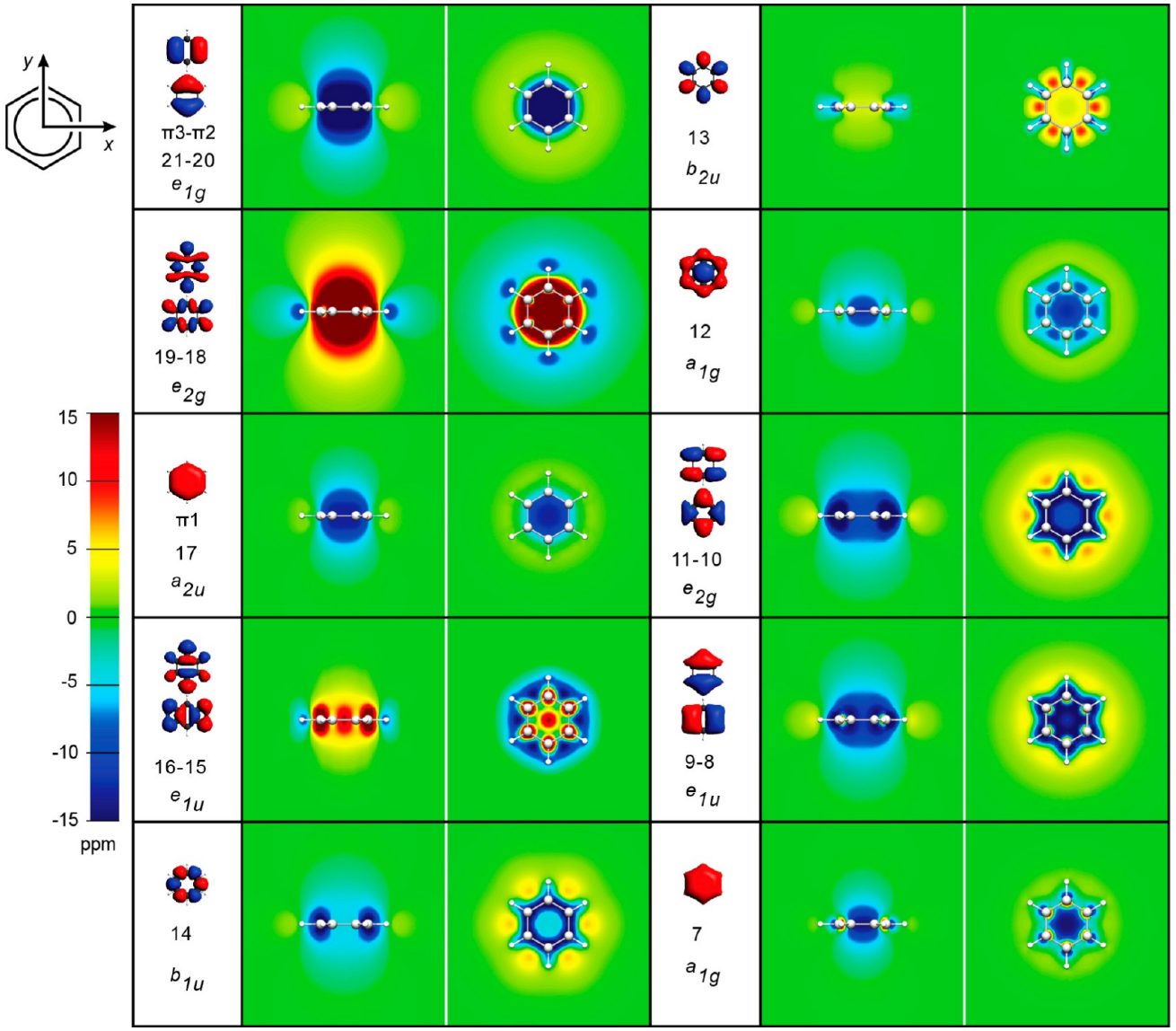

Figure 1. Contour maps of MO contributions to the *z*-component of the IMF $\mathbf{B}_z^{ind}$ (ppm) of benzene on the *yz* and *xy* planes. Blue areas represent diatropicity and red paratropicity. Orbitals are numbered with increasing energy.

can be called CMO-IMF. Visualizations of CMO-IMF provide a clear view of the spatial extension, shape, and magnitude of shielding and deshielding areas within the vicinity of the molecule, originating from the induced currents of individual MOs, in response to an applied magnetic field. CMO-IMF combines the analytic insight provided by the dissection of chemical shielding to individual canonical MO contributions, along with the visual comprehension of the magnetic response in the whole molecular space. Therefore, CMO-IMF can be applied for the in-depth investigation of various types of electron delocalization in which other NICS-based methods do not present sufficient information for deducing unambiguous conclusions. We first apply this method to the archetypical paradigms of aromatic and antiaromatic species, benzene and cyclobutadiene, and to borazine, in which the degree of aromaticity is controversial, in order to investigate the delocalization of each valence MO and to evaluate their contribution to the aromatic character of these systems.

COMPUTATIONAL DETAILS

Geometry optimizations of benzene (D_{6h}), cyclobutadiene (D_{2h}), and borazine (D_{3h}) were performed at the B3LYP/6-311++G(d,p) level of theory[35,36] using Gaussian 03W.[37] Chemical shielding calculations were performed at the PW91/TZ2P level,[38] employing the GIAO method as implemented by Schreckenbach[39] in ADF package.[40]

The center of each molecule was placed on the origin of the Cartesian axes with the molecular plane lying on the *xy* plane. Chemical shieldings were computed in two-dimensional grids of points ranging from −6 to +6 Å with a step of 0.2 Å in each direction, on the molecular plane and on a plane perpendicular to it. The IMF is derived from the chemical shielding tensor. The relation of the chemical shielding tensor $\boldsymbol{\sigma}(\boldsymbol{r})$ with the magnetic field, $\mathbf{B}^{ind}$, which is induced when an external magnetic field, $\mathbf{B}^{ext}$, is applied perpendicular to the molecular ring plane, is given by following equation

$$B_i^{ind}(r) = -\sigma_{ij}(r)B_j^{ext}$$

dx.doi.org/10.1021/jp411410r | J. Phys. Chem. A XXXX, XXX, XXX−XXX

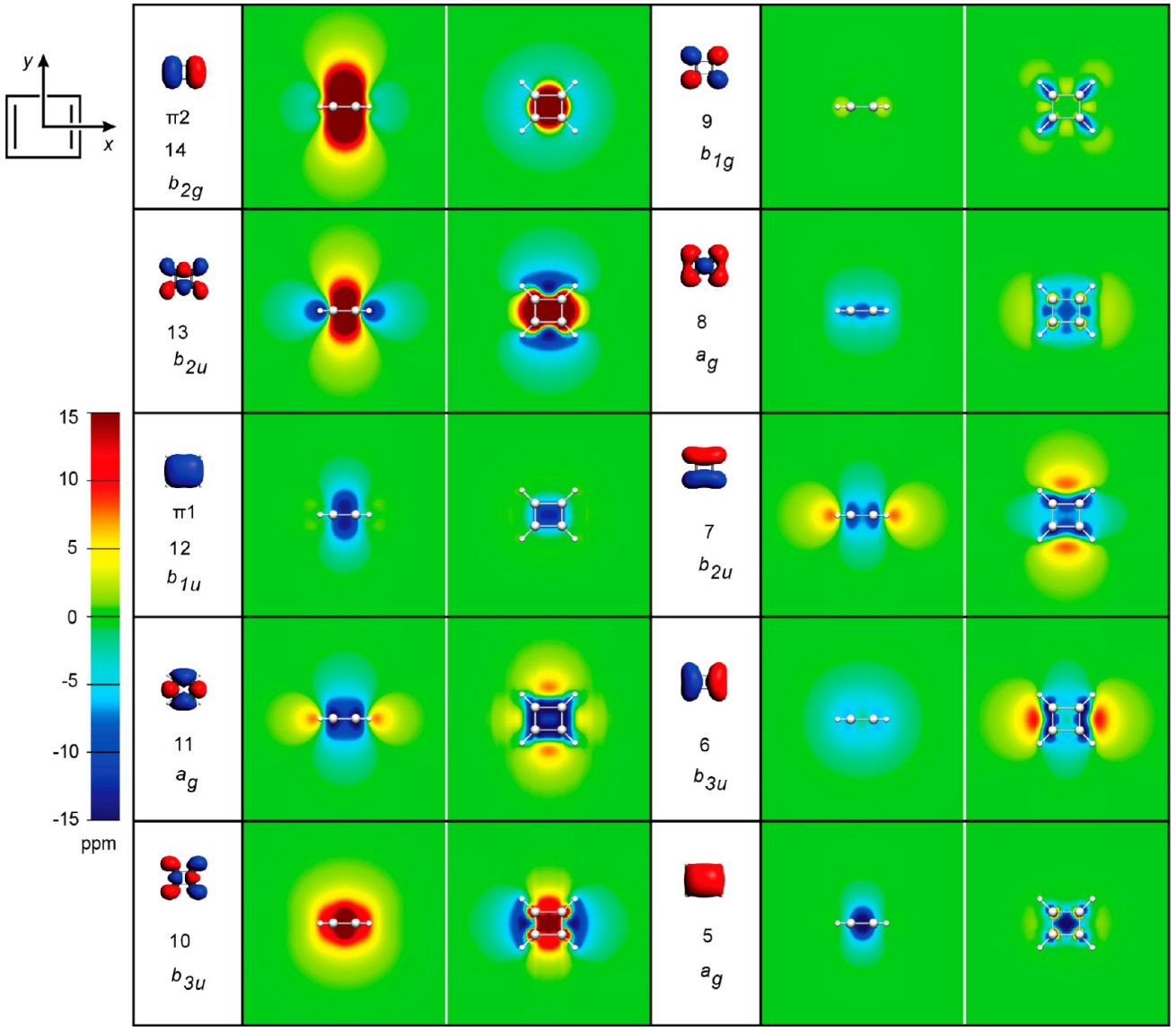

Figure 2. Contour maps of MO contributions to the *z*-component of the IMF $\mathbf{B}_z^{ind}$ (ppm) of cyclobutadiene on the *yz* and *xy* planes. Blue areas represent diatropicity and red paratropicity. Orbitals are numbered with increasing energy.

Chemical shielding is derived as a 3 × 3 tensor in which the columns denote indexes of the IMF, while the rows denote indexes of the applied magnetic field. The isotropic value of the chemical shielding is the trace of the shielding tensor, which is one-third of the sum of the diagonal symmetric components. If the molecular plane lies on the *xy* Cartesian plane, then the first, second, and third rows represent the IMF when the external field is applied on the *x*, *y*, and *z* Cartesian axes, respectively. Therefore, the σ_{31}, σ_{32}, and σ_{33} components of the chemical shielding tensor at a specific point are equal to the *x*-, *y*-, and *z*-components, respectively, of the vector of the IMF, when the external field is applied perpendicular to the molecular plane, $\vec{B}^{ind} = (\sigma_{31}, \sigma_{32}, \sigma_{33})$. Hence, the *z*-component of the induced field, $\mathbf{B}_z^{ind}$, is equivalent to $NICS_{zz}$ or σ_{33}. Assuming that the magnitude of the external field is $|\mathbf{B}^{ext}| = 1.0$ T, the results of the induced field are given in μT of the external field or ppm of the shielding tensor. The IMFs are visualized as vectors of the IMF and as contour maps of the magnitude and of the *z*-component of the IMF for each valence MO. Input preparation, output processing, and visualization were performed with MIMAF program developed by our group.[41]

RESULTS AND DISCUSSION

In the following section, the contributions of each occupied valence MO to the IMF are discussed for the three molecules under study. Contour maps of the *z*-component of the IMF for each valence orbital of benzene, cyclobutadiene, and borazine are presented in Figures 1−3. Vectors of the IMF, contour maps of its magnitude, and contour maps of $NICS_{iso}$ for each valence orbital of benzene (Figures S1 and S2,), cyclobutadiene (Figures S3 and S4,), and borazine (Figures S5 and S6,) are provided as Supporting Information. The isocontour maps of the contributions of π , σ, and core subsets of MOs to the *z*-component of the IMF for all molecules are shown in Figure 4. Vectors of the IMF, contour maps of its magnitude (Figure S7,), and contour maps of $NICS_{iso}$ (Figure S8,) of π and σ subsets of MOs are provided as Supporting Information.

π Orbitals. The low-energy fully delocalized π-HOMO−1 orbital (π1) of each molecule, which is MO 17 (a_{2u}) of benzene

dx.doi.org/10.1021/jp411410r | J. Phys. Chem. A XXXX, XXX, XXX−XXX

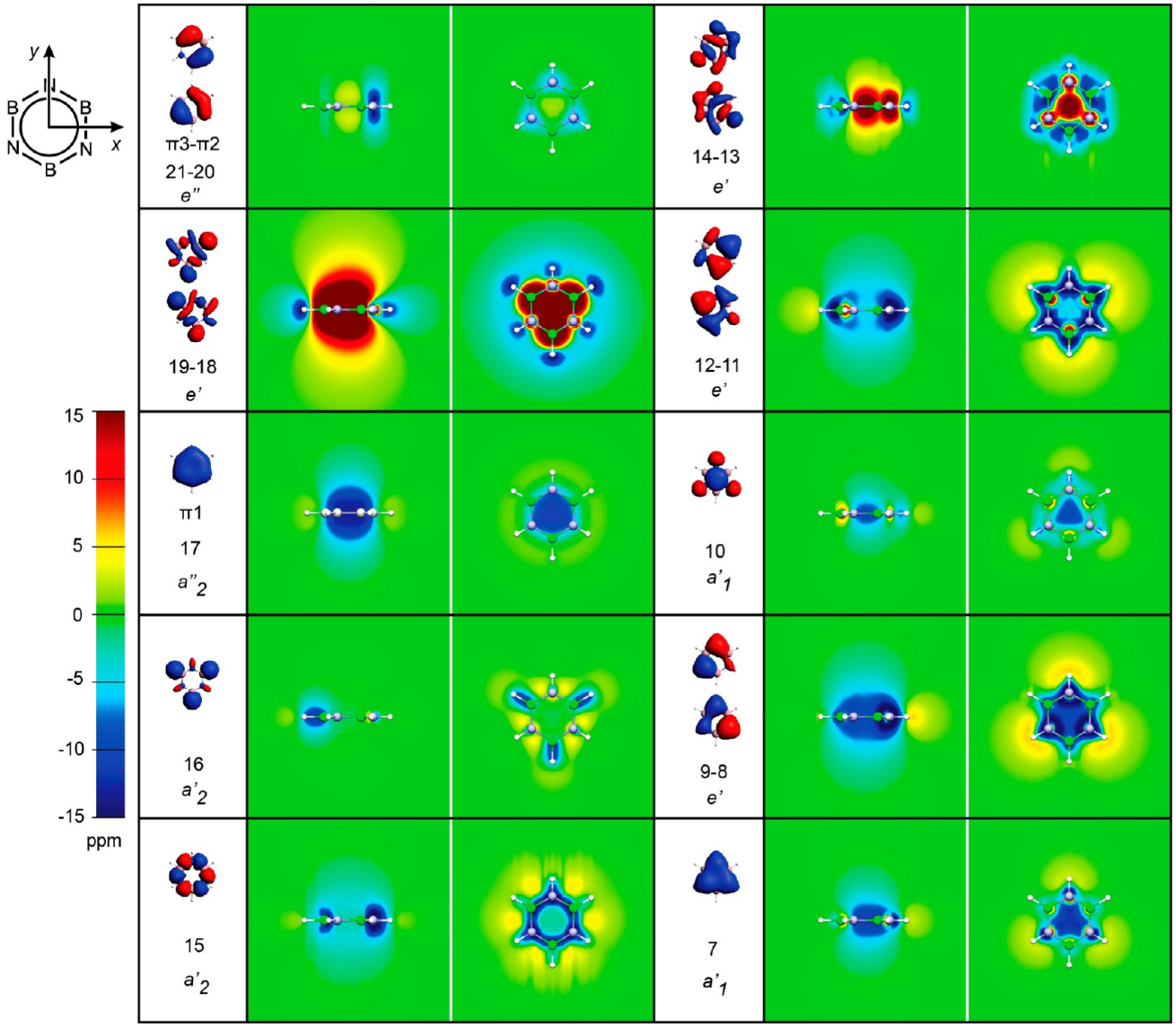

Figure 3. Contour maps of MO contributions to the *z*-component of the IMF $\mathbf{B}_z^{ind}$ (ppm) of borazine on the *yz* and *xy* planes. Blue areas represent diatropicity and red paratropicity. Orbitals are numbered with increasing energy.

in Figure 1, MO 12 (b_{1u}) of cyclobutadiene in Figure 2, and MO 17 (a_2'') of borazine in Figure 3, exhibits a similar diatropic magnetic response. These three MOs show a strong diatropic region inside of the ring with moderate spatial extension perpendicular to the ring and a very weak, almost negligible, paratropic circular region outside of the ring. The diatropic region on the ring plane adopts the shape of the corresponding orbital in all molecules. Thus, the HOMO−1 π orbitals (π1) show the same moderate diatropic response in the three molecules, denoting similar weak electron delocalization.

The magnetic response of π-HOMO orbitals of benzene (π3−π2) and cyclobutadiene (π2) is much stronger than the response of the π-HOMO−1 orbitals (π1). In benzene, the four electrons in doubly degenerate π-HOMO orbitals, π3−π2 in Figure 1, exhibit a strong and long-ranged diatropic response. On the molecular plane, the diatropic region surrounds the ring, whereas a weak circular paratropic region is observed outside of the ring with the hydrogen atoms located inside of it. In cyclobutadiene, the two electrons of the π-HOMO orbital, π2 in Figure 2, exhibit a strong and long-ranged paratropic response. On the molecular plane of cyclobutadiene, the shape of the paratropic region is elongated parallel to the short C−C bonds. Unlike benzene and cyclobutadiene, in borazine, the four electrons of the doubly degenerate π-HOMO orbitals, π3−π2 in Figure 3, exhibit a very weak magnetic response, with short-ranged diatropic areas localized around nitrogen atoms, whereas no magnetic response is observed at boron centers. Inside of the ring, a very weak and short-ranged paratropic region is observed.

The well-known magnetic response of the total π-system of the three molecules is due to the sum of π-MO contributions and is presented in Figure 4. Benzene's π-system presents a strong and long-range diatropic response inside of and above the molecular ring and a weak short-range paratropic region outside of the ring, with the hydrogen atoms lying inside of it, in agreement with the early Pople's ring current model. Cyclobutadiene's π-system presents a strong and long-range paratropic response inside of and above the molecular ring and a very weak and short-range diatropic region outside of the ring, with the hydrogen atoms lying inside of it. In borazine, the π-

dx.doi.org/10.1021/jp411410r | J. Phys. Chem. A XXXX, XXX, XXX−XXX

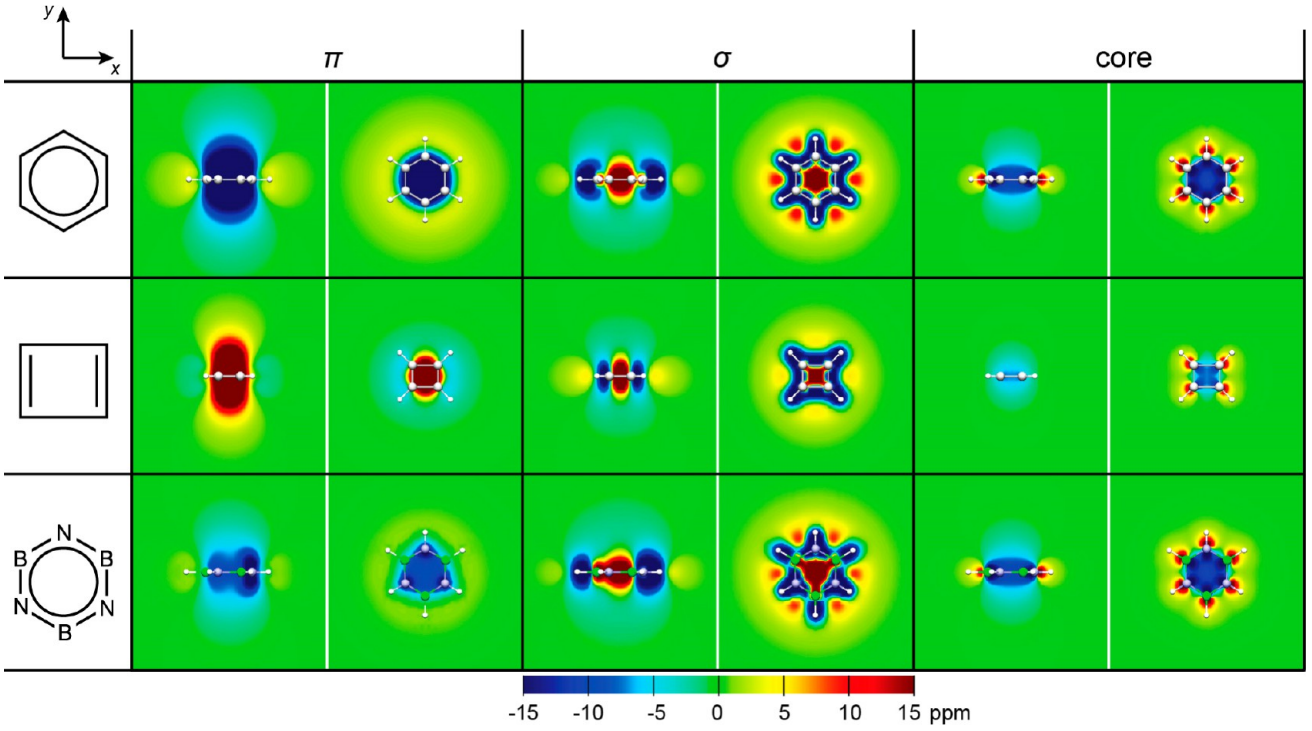

Figure 4. Contour maps of π, σ, and core contributions to the z-component of the IMF $\mathbf{B}_z^{ind}$ (ppm) of (A) benzene, (B) cyclobutadiene, and (C) borazine on the yz and xy planes. Blue areas represent diatropicity and red paratropicity.

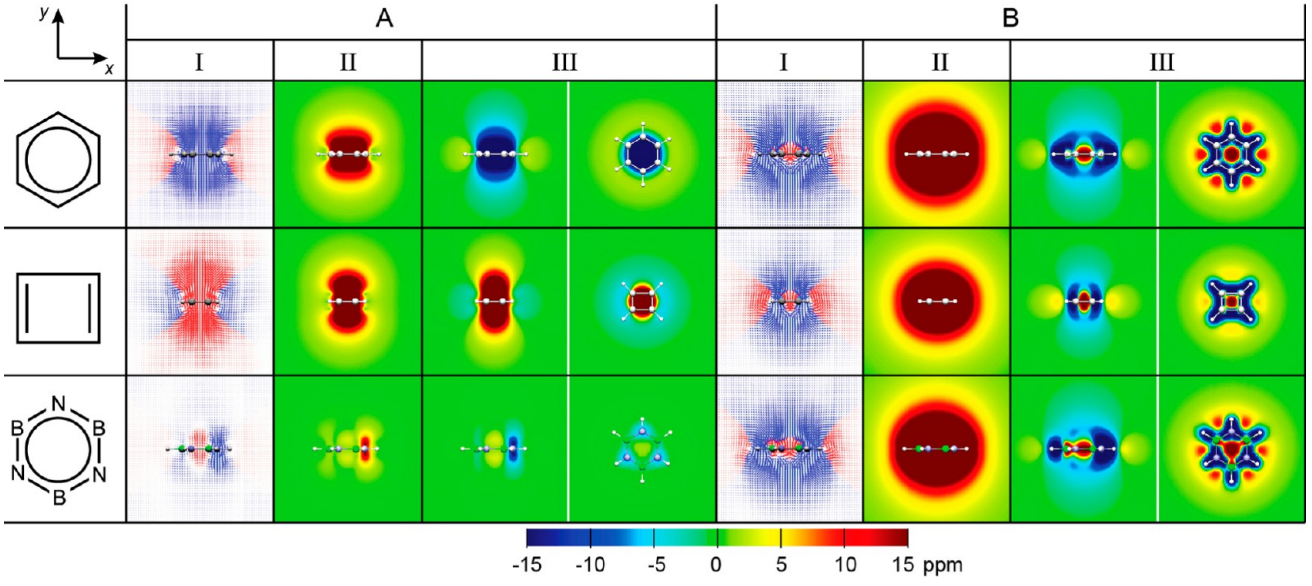

Figure 5. (I) Vectors of the IMF $\mathbf{B}^{ind}$, (II) contour maps of the magnitude of the IMF $|\mathbf{B}^{ind}|$ (ppm) on the yz plane, and (III) contour maps of the z-component of the IMF $\mathbf{B}_z^{ind}$ (ppm) on the yz and xy planes of (A) the HOMO and (B) the rest of valence orbitals for benzene, cyclobutadiene, and borazine.

system presents a diatropic response, which is much weaker and less extended than benzene's π-response. Strong diatropic areas are observed in the vicinity of nitrogen atoms, whereas the diatropic response weakens in the region of boron atoms. On the ring plane, the diatropic region shows a curved triangular shape. Outside of borazine's ring, a very weak and short-ranged paratropic region is observed. Hydrogen atoms bonded to boron atoms are located inside of the paratropic region, while those bonded to nitrogen atoms are located on the nodal plane between diatropic and paratropic regions.

As our method allows the visualization of the magnetic response of any subset of MOs, the magnetic response of π-HOMO versus the response of the sum of the rest of the valence orbitals for each molecule is visualized in Figure 5A and B. It is clearly shown that the magnetic response of all valence orbitals except HOMO is almost identical among the three molecules under study. The differentiation of the total magnetic response originates solely from the HOMO π orbitals, which exhibit three different responses that are representative of aromatic, antiaromatic, and nonaromatic character. Thus,

dx.doi.org/10.1021/jp411410r | J. Phys. Chem. A XXXX, XXX, XXX−XXX

Table 1. MO Contributions to $NICS_{zz}$ and $NICS_{iso}$ at Ring Centers of Benzene, Cyclobutadiene, and Borazine[a]

benzene			cyclobutadiene			borazine		
MO	$NICS_{zz}$	$NICS_{iso}$	MO	$NICS_{zz}$	$NICS_{iso}$	MO	$NICS_{zz}$	$NICS_{iso}$
21−20 (e_{1g}) π3−π2	−23.4	−9.4	14 (b_{2g}) π2	72.1	25.9	21−20 (e'') π3−π2	0.8	−0.9
19−18 (e_{2g})	67.6	28.2	13 (b_{2u})	77.8	34.2	19−18 (e')	22.9	9.2
17 (a_{2u}) π1	−12.8	−13.8	12 (b_{1u}) π1	−12.9	−21.7	17 (a_2'') π1	−11.0	−11.5
16−15 (e_{1u})	14.0	10.2	11 (a_g)	−11.7	4.8	16 (a_2')	−0.9	−0.3
14 (b_{1u})	−4.2	5.9	10 (b_{3u})	34.5	17.8	15 (a_2')	−2.4	4.0
13 (b_{2u})	2.9	1.6	9 (b_{1g})	−0.4	−0.4	14−13 (e')	11.3	7.2
12 (a_{1g})	−12.3	−7.6	8 (a_g)	−9.7	−6.9	12−11 (e')	−2.0	−1.6
11−10 (e_{2g})	−8.8	−5.0	7 (b_{2u})	−6.7	−3.1	10 (a_1')	−9.6	−6.9
9−8 (e_{1u})	−11.4	−4.8	6 (b_{3u})	−1.6	−0.4	9−8 (e')	−4.7	−2.2
7 (a_{1g})	−14.4	−8.7	5 (a_g)	−19.8	−17.8	7 (a_1')	−11.7	−6.5
π	−36.2	−23.1	π	59.2	4.2	π	−9.2	−13.2
σ	33.3	19.6	σ	62.6	28.4	σ	30.1	15.5
core	−10.8	−3.9	core	−7.2	−3.0	core	−10.6	−3.8
total	−13.7	−7.4	total	114.6	29.6	total	10.3	−1.5

[a]Values are in ppm calculated at the PW91/TZ2P level of theory.

benzene's π-HOMO orbitals (π3−π2) show strong and long-range diatropic response, originating from diatropic ring currents that characterize aromatic molecules. The strong and long-range paratropic magnetic response of cyclobutadiene's π-HOMO orbital (π2) represents paratropic ring currents that characterize antiaromatic molecules. In borazine, the minimal magnetic response of π-HOMO orbitals (π3−π2) denotes that no ring current originates from these electrons. Instead, strong short-ranged diatropic areas in the vicinity of nitrogen atoms, along with the absence of the magnetic response at boron centers, indicate that the π-HOMO electrons are firmly localized on nitrogen centers. The moderate diatropic response of the total π-system of borazine originates from the π-HOMO−1 orbital (π1), which exhibits the same magnetic response with the corresponding orbitals of benzene and cyclobutadiene. Hence, borazine is classified as nonaromatic.

σ Orbitals. In this section, the magnetic response of each σ-orbital is discussed. As shown in Figures 1−3, the general trend is that low-energy σ orbitals with few nodes show diatropic response, while high-energy σ orbitals with many angular nodes show paratropic response. Furthermore, σ orbitals with similar nodal patterns among the three molecules under study present similar magnetic response.

The highest occupied degenerate σ orbitals of benzene (MOs 19−18, e_{2g} in Figure 1) show a very strong and long-range paratropic response. In fact, these orbitals show the strongest and more extended magnetic response among all orbitals. The shape of the paratropic region on the molecular plane of benzene is hexagonal and extends outside of the carbon ring. The hydrogens are located inside of a diatropic region, which encircles the paratropic region. The magnetic response of the corresponding orbitals of cyclobutadiene (MO 13, b_{2u} in Figure 2) and borazine (MOs 19−18, e′ in Figure 3) is similar. In cyclobutadiene, the paratropic region is elongated parallel to the long C−C bonds, following the symmetry of the MO. In borazine, the paratropic response is stronger in the vicinity of boron atoms, while nitrogen atoms are barely surrounded by a diatropic region. Paratropic response also exhibits the next set of MOs with many angular nodes, that is, MOs 16−15 (e_{1u}) in Figure 1 of benzene, MO 10 (b_{3u}) in Figure 2 of cyclobutadiene, and MOs 14−13 (e′) in Figure 3 of borazine. The paratropic response inside of the ring is stronger in cyclobutadiene but has a moderate extension perpendicular to the molecular plane in all molecules. The paratropic region on the molecular plane of cyclobutadiene is elongated parallel to the short C−C bonds. On the molecular plane of benzene, it is cyclic and confined inside of the ring and around carbon atoms. In borazine, the paratropic region inside of the ring is also cyclic, and it extends to encapsulate nitrogen atoms, while the boron atoms are located inside of the diatropic region. The above two sets of MOs are responsible for the paratropic magnetic response of the total σ-system of benzene, cyclobutadiene, and borazine, as shown in Figure 4. The MOs involved and located along the C−H (B−H and N−H in borazine) σ-bonds, that is, MO 13 (b_{1u}) of benzene in Figure 1, MO 9 (b_{1g}) of cyclobutadiene in Figure 2, and MO 16 (a_2') of borazine in Figure 3, exhibit the weakest and almost negligible magnetic response.

The rest of σ orbitals exhibit diatropic magnetic response. MOs involved and located along the C−C (B−N in borazine) σ-bonds, that is, MO 14 (b_{1u}) of benzene in Figure 1, MO 11 (a_g) of cyclobutadiene in Figure 2, and MO 15 (a_2') of borazine in Figure 3, show a moderate diatropic response that is stronger along the C−C (B−N in borazine) framework and weakens inside of the ring. The in-plane MOs with overlapping lobes inside of the ring, MO 12 (a_{1g}) of benzene in Figure 1, MO 8 (a_g) of cyclobutadiene in Figure 2, and MO 10 (a_1') of borazine in Figure 3, show a weak and short-range diatropic response inside of the ring that weakens along the C−C (B−N in borazine) framework. On the molecular plane of borazine, the magnetic response of MO 10 has a triangular shape with its vertexes pointing at nitrogen atoms. The σ MOs 10−11 (e_{2g}) in benzene in Figure 1 and 11−12 (e′) in borazine in Figure 3 have two nodal planes, while cyclobutadiene does not have a corresponding orbital. These orbitals exhibit a moderate diatropic response that is augmented along the molecular framework and weakens significantly inside of the ring. Similar moderate diatropic magnetic response exhibits the low-energy σ orbitals with one nodal plane, that is, MOs 9−8 (e_{1u}) of benzene in Figure 1, MO 7 (b_{2u}) and MO 6 (b_{3u}) in cyclobutadiene in Figure 2, and MOs 9−8 (e′) in borazine in Figure 3. Finally, the fully delocalized lowest-energy σ orbitals, MO 7 (a_{1g}) of benzene in Figure 1, MO 5 (a_g) of cyclobutadiene in Figure 2, and MO 7 (a_1') of borazine in Figure 3, exhibit a weak and short-range diatropic response confined inside of the ring.

dx.doi.org/10.1021/jp411410r | J. Phys. Chem. A XXXX, XXX, XXX−XXX

Visualizations of MO contributions to the IMF can clarify the interpretation of CMO-NICS values shown in Table 1. The fully delocalized lowest-energy σ orbitals have very high diatropic $NICS_{zz}$ values; MO 5 (a_g) of cyclobutadiene has a $NICS_{zz}$ value (−19.8 ppm) comparable to $NICS_{zz}$ of benzene's π-HOMO orbitals $\pi3-\pi2$ (−23.4 ppm). The in-plane delocalized σ orbitals, MO 12 (a_{1g}) of benzene, MO 8 (a_g) of cyclobutadiene, and MO 10 (a_1') of borazine, also exhibit very high $NICS_{zz}$ values. These values imply that low-energy delocalized σ orbitals have significant contribution to the total diatropic response of the molecule, comparable to the π response. However, visualizations of the z-component of the IMF reveal that the magnetic response of these orbitals is short-ranged with small spatial extension, denoting that it originates from localized electrons.

On the other hand, orbitals with one or two nodal planes involved in C−C bonds (B−N in borazine) (MOs 9−8 and MOs 11−10 of benzene, MOs 6−7 of cyclobutadiene, MOs 9−8 and MOs 12−11 of borazine) show a more extended diatropic response than the fully delocalized and in-plane σ orbitals, although they have smaller $NICS_{zz}$ values at ring centers. This extended diatropic response, which is augmented along the carbon framework, is indicative of less localized σ-electrons. These findings suggest that interpretation of CMO-NICS values may not be straightforward because single-point calculations at ring centers may lead to misinterpretations about an orbital's overall magnetic response.

The total σ-system, which resulted from the sum of contributions of all σ-MOs, presents similar magnetic response in the three molecules under study, as is shown in Figure 4. A strong paratropic region is observed inside of the ring, extending approximately to 1.5 Å above the ring. A strong diatropic region with the same extension perpendicular to the ring is tracking the molecular framework and encapsulating all ring atoms except those of boron in borazine lying inside of the paratropic region. Outside of the molecular framework, a weak circular and short-ranged paratropic area is observed, which presents stronger values between hydrogen atoms. The contour plots of the z-component of the IMF of the σ subset of MOs (Figure 4) can clarify the interpretation of LMO-NICS indexes. Thus, the out-of-plane component of NICS of the σ-system in the center of the ring, $NICS(0)_{\sigma zz}$ for cyclobutadiene (62.6 ppm), is almost the double of the same index in benzene (33.3 ppm) and borazine (30.1 ppm). However, $\mathbf{B}_z^{ind}$ maps reveal the same magnetic response of the σ-system in all three molecules.

SUMMARY AND CONCLUSIONS

The dissection of the IMF into contributions from each MO employing the GIAO method can provide valuable insight about electron delocalization. Visualizations of CMO-IMF provide a clear view of the spatial extension, shape, and magnitude of shielding and deshielding areas within the vicinity of the molecule, originating from the induced currents of each MO in response to the applied magnetic field.

The two sets of highest-energy occupied MOs of benzene and cyclobutadiene exhibit the strongest and spatially more extended magnetic response and dominate against the other MOs. On the contrary, the HOMO of borazine presents a negligible magnetic response with short-ranged diatropic areas in the vicinity of nitrogen atoms, clearly portraying the localization of borazine's π-HOMO ($\pi3-\pi2$) electrons on nitrogen centers.

The rest of the orbitals show a moderate or weak magnetic response. The low-energy fully delocalized π orbitals ($\pi1$) exhibit the same moderate magnetic response among the molecules under study. It was found that σ orbitals with similar nodal patterns exhibit similar magnetic response, despite the variations that they may present in their $NICS_{zz}$ values. Our analysis revealed that low-energy fully delocalized and in-plane σ orbitals, which have large diatropic $NICS_{zz}$ values on the ring center, present a short-range diatropic response that is attributed to localized electrons. Furthermore, it was found that although σ orbitals with one or two nodal planes have smaller diatropic $NICS_{zz}$ values, they present a more extended magnetic response that is indicative of less localized electrons on the ring framework. These findings illustrate that CMO-NICS values at ring centers do not provide sufficient information about an orbital's overall magnetic response and are not always representative of the degree of electron delocalization.

The differentiation of the total magnetic response, and hence the evaluation of aromaticity, is attributed exclusively to π-HOMOs because the magnetic response of the sum of the rest of the valence orbitals is identical among the molecules under study. Benzene's aromaticity is attributed to the long-range diatropic response of the four electrons occupying the double degenerate π-HOMO ($\pi3-\pi2$). The antiaromaticity of cyclobutadiene is attributed to the long-range paratropic response of the two electrons that occupy the nondegenerate π-HOMO ($\pi2$). Borazine is classified as nonaromatic, given that the four electrons that occupy the doubly degenerate π-HOMO ($\pi3-\pi2$) are found to be strongly localized, as they present a negligible magnetic response.

It was shown that CMO-IMF is a valid method for the investigation of electron delocalization and the evaluation of aromaticity as it combines the analytic insight provided by the dissection of the chemical shielding to individual MOs contributions along with the visual comprehension of the magnetic response in the whole molecular space. Hence, it could be applied to species presenting multiple types of aromaticity, such as σ, radial, and metal aromaticity. Such calculations are currently being carried out by our team. Furthermore, visualizations of CMO-IMF could be even more deeply dissected into interactions between occupied and unoccupied MOs, providing information about the physical origins of the magnetic response.

ASSOCIATED CONTENT

Supporting Information

Vectors of the induced magnetic field, contour maps of the magnitude of the induced magnetic field, contour maps of $NICS_{iso}$ for total magnetic response for π, σ, and core subsets of MOs and for each valence molecular orbital of benzene, cyclobutadiene, and borazine, and the full citation of ref 37. This material is available free of charge via the Internet at http://pubs.acs.org.

AUTHOR INFORMATION

Corresponding Authors

*E-mail: sigalas@chem.auth.gr. Phone: +302310997815. Fax: +2310997738 (M.P.S.).
*E-mail: nicharis@chem.auth.gr. Phone: +302310997754. Fax: +302310997689 (N.D.C.).

Notes

The authors declare no competing financial interest.

■ ACKNOWLEDGMENTS

This research has been co-financed by the European Union (European Social Fund − ESF) and Greek national funds through the Operational Program "Education and Lifelong Learning" of the National Strategic Reference Framework (NSRF) - Research Funding Program: Thales. Investing in knowledge society through the European Social Fund.

■ REFERENCES

(1) Hückel, E. Zur Quantenthorie der Doppelbindung. *Z. Phys* **1930**, *60*, 423−456.
(2) Schleyer, P.; von, R. Introduction: Aromaticity. *Chem. Rev.* **2001**, *101*, 1115−1118.
(3) Schleyer, P.; von, R. Introduction: Delocalization—Pi and Sigma. *Chem. Rev.* **2005**, *105*, 3433−3435.
(4) Gonthier, J. F.; Steinmann, S. N.; Wodrich, M. D.; Corminboeuf, C. Quantification of "Fuzzy" Chemical Concepts: A Computational Perspective. *Chem. Soc. Rev.* **2012**, *41*, 4671−4687.
(5) Stanger, A. What Is...Aromaticity: A Critique of the Concept of Aromaticity—Can It Really Be Defined? *Chem. Commun.* **2009**, *15*, 1939−1947.
(6) Pople, J. A. Molecular Orbital Theory of Aromatic Ring Currents. *Mol. Phys.* **1958**, *1*, 175−180.
(7) Chen, Z.; Wannere, C. S.; Corminboeuf, C.; Puchta, R.; Schleyer, P. v. R. Nucleus-Independent Chemical Shifts (NICS) As an Aromaticity Criterion. *Chem. Rev.* **2005**, *105*, 3842−3888.
(8) Islas, R.; Martínez-Guajardo, G.; Jiménez-Halla, J. O. C.; Solà, M.; Merino, G. Not All That Has a Negative Nics Is Aromatic: The Case of the H-Bonded Cyclic Trimer of HF. *J. Chem. Theory Comput.* **2010**, *6*, 1131−1135.
(9) Torres, J. J.; Islas, R.; Osorio, E.; Harrison, J. G.; Tiznado, W.; Merino, G. Is Al_2Cl_6 Aromatic? Cautions in Superficial NICS Interpretation. *J. Phys. Chem. A* **2013**, *117*, 5529−5533.
(10) Castro, A. C.; Osorio, E.; Jiménez-Halla, J. O. C.; Matito, E.; Tiznado, W.; Merino, G. Scalar and Spin−Orbit Relativistic Corrections to the NICS and the Induced Magnetic Field: The Case of the E122−Spherenes (E = Ge, Sn, Pb). *J. Chem. Theory Comput.* **2010**, *6*, 2701−2705.
(11) Lazzeretti, P. Assessment of Aromaticity via Molecular Response Properties. *Phys. Chem. Chem. Phys.* **2004**, *6*, 217−223.
(12) Schleyer, P. v. R.; Manoharan, M.; Wang, Z.-X.; Kiran, B.; Jiao, H.; Puchta, R.; Eikema Hommes, N. J. R. Dissected Nucleus-Independent Chemical Shift Analysis of π-Aromaticity and Antiaromaticity. *Org. Lett.* **2001**, *3*, 2465−2468.
(13) Schleyer, P. v. R.; Jiao, H.; Eikema Hommes, N. J. R.; Malkin, V. G.; Malkina, O. An Evaluation of the Aromaticity of Inorganic Rings: Refined Evidence from Magnetic Properties. *J. Am. Chem. Soc.* **1997**, *119*, 12669−12670.
(14) Kutzelnigg, W. Theory of the Magnetic Susceptibility and NMR Chemical Shift in Terms of Localized Quantities. *Isr. J. Chem.* **1980**, *19*, 193−200.
(15) Pipek, J.; Mezey, P. J. A Fast Intrinsic Localization Procedure Applicable for Ab Initio and Semiempirical Linear Combination of Atomic Orbital Wave Functions. *J. Chem. Phys.* **1989**, *90*, 4916−4926.
(16) Fallah-Bagher-Shaidaei, H.; Wannere, C. S.; Corminboeuf, C.; Puchta, R.; Schleyer, P. v. R. Which NICS Aromaticity Index for Planar π Rings Is Best? *Org. Lett.* **2006**, *8*, 863−866.
(17) Heine, T.; Schleyer, P. v. R.; Corminboeuf, C.; Seifert, G.; Reviakine, R.; Weber, J. Analysis of Aromatic Delocalization: Individual Molecular Orbital Contributions to Nucleus-Independent Chemical Shifts. *J. Phys. Chem. A* **2003**, *107*, 6470−6475.
(18) Ditchfield, R. Self-Consistent Perturbation Theory of Diamagnetism. *Mol. Phys.* **1974**, *27*, 789−807.
(19) Chen, Z.; Corminboeuf, C.; Heine, T.; Bohmann, J.; Schleyer, P. v. R. Do All-Metal Antiaromatic Clusters Exist? *J. Am. Chem. Soc.* **2003**, *125*, 13930−13931.
(20) Wodrich, M. D.; Corminboeuf, C.; Park, S.; Schleyer, P. v. R. Double Aromaticity in Monocyclic Carbon, Boron, And Borocarbon Rings Based on Magnetic Criteria. *Chem.—Eur. J.* **2007**, *13*, 4582−4593.
(21) Wannere, C. S.; Corminboeuf, C.; Wang, Z. X.; Wodrich, M. D.; King, R. B.; Schleyer, P. v. R. Evidence for d Orbital Aromaticity in Square Planar Coinage Metal Clusters. *J. Am. Chem. Soc.* **2005**, *127*, 5701−5705.
(22) Corminboeuf, C.; King, R. B.; Schleyer, P. v. R. Implications of Molecular Orbital Symmetries and Energies for the Electron Delocalization of Inorganic Clusters. *Chem. Phys. Chem.* **2007**, *8*, 391−398.
(23) Corminboeuf, C.; Heine, T.; Seifert, G.; Schleyer, P. v. R.; Weber, J. Induced Magnetic Fields in Aromatic [n]-Annulenes—Interpretation of NICS Tensor Components. *Phys. Chem. Chem. Phys.* **2004**, *6*, 273−276.
(24) Steiner, E.; Fowler, P. W. On the Orbital Analysis of Magnetic Properties. *Phys. Chem. Chem. Phys.* **2004**, *6*, 261−272.
(25) Klod, S.; Kleinpeter, E. Ab Initio Calculation of the Anisotropy Effect of Multiple Bonds and the Ring Current Effect of Arenes—application in Conformational and Configurational Analysis. *J. Chem. Soc., Perkin Trans. 2* **2001**, 1893−1898.
(26) Karadakov, B. P.; Horner, E. K. Magnetic Shielding in and around Benzene and Cyclobutadiene: A Source of Information about Aromaticity, Antiaromaticity, And Chemical Bonding. *J. Phys. Chem. A* **2013**, *117*, 518−523.
(27) Merino, G.; Heine, T.; Seifert, G. The Induced Magnetic Field in Cyclic Molecules. *Chem.—Eur. J.* **2004**, *10*, 4367−4371.
(28) Papadopoulos, A. G.; Charistos, N. D.; Sigalas, M. P. Aromaticity Variation in BN Substituted Triphenylene: A Theoretical Study. *AIP Conf. Proc.* **2012**, *1504*, 1223−1226.
(29) Muñoz-Castro, A. On the Magnetic Behavior of Spherical Aromatic Compounds. Insights from the closo-$[B_{12}H_{12}]$ Cluster through Chemical Shift Tensor Maps. *Chem. Phys. Lett.* **2013**, *555*, 282−285.
(30) Muñoz-Castro, A. Magnetic Response Properties of Coinage Metal Macrocyles. Insights into the Induced Magnetic Field through the Analysis of $[Cu_5(Mes)_5]$, $[Ag_4(Mes)_4]$, and $[Au_5(Mes)_5]$ (Mes = 2,4,6-$Me_3C_6H_2$). *J. Phys. Chem. C* **2012**, *116*, 17197−17203.
(31) Heine, T.; Islas, R.; Merino, G. σ and π Contributions to the Induced Magnetic Field: Indicators for the Mobility of Electrons in Molecules. *J. Comput. Chem.* **2007**, *28*, 302−309.
(32) Islas, R.; Heine, T.; Merino, G. The Induced Magnetic Field. *Acc. Chem. Res.* **2012**, *45*, 215−228.
(33) Islas, R.; Chamorro, E.; Robles, J.; Heine, T.; Santos, J. C.; Merino, G. Borazine: To Be or Not to Be Aromatic. *Struct. Chem.* **2007**, *18*, 833−839.
(34) Islas, R.; Heine, T.; Ito, K.; Schleyer, P. v. R.; Merino, G. Boron Rings Enclosing Planar Hypercoordinate Group 14 Elements. *J. Am. Chem. Soc.* **2007**, *129*, 14767−14774.
(35) Becke, A. D. Density-Functional Thermochemistry. III. The Role of Exact Exchange. *J. Chem. Phys.* **1993**, *98*, 5648−5652.
(36) Lee, C.; Yang, W.; Parr, R. G. Development of the Colle−Salvetti Correlation-Energy Formula into a Functional of the Electron Density. *Phys. Rev. B* **1988**, *37*, 785−789.
(37) Frisch, M. J.; Trucks, G. W.; Schlegel, H. B.; Scuseria, G. E.; Robb, M. A.; Cheeseman, J. R.; Montgomery, J. A., Jr.; Vreven, T.; Kudin, K. N.; Burant, J. C.; et al. *Gaussian 03*, Revision E.01; Gaussian, Inc.: Pittsburgh, PA, 2003.
(38) Perdew, J. P.; Burke, K.; Wang, Y. Generalized Gradient Approximation for the Exchange−Correlation Hole of a Many-Electron System. *Phys. Rev. B* **1996**, *54*, 16533.
(39) Schreckenbach, G.; Ziegler, T. Calculation of NMR Shielding Tensors Using Gauge-Including Atomic Orbitals and Modern Density Functional Theory. *J. Phys. Chem.* **1995**, *99*, 606.

(40) *Amsterdam Density Functional (ADF) Code*, release 2010; SCM, Theoretical Chemistry, Vrije Universiteit: Amsterdam, The Netherlands, 2010; http://www.scm.com.
(41) Charistos, N. D.; Sigalas, M. P. *MIMAF (Molecular Induced MAgnetic Fields)*; Laboratory of Applied Quantum Chemistry, Department of Chemistry, Aristotle University of Thessaloniki: Greece, 2010.